Journal of Coordination Chemistry

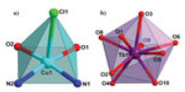

ISSN: (Print) (Online) Journal homepage: www.tandfonline.com/journals/gcoo20

The effect of substituents on the reactivity of dichloridotriphenylphosphinoruthenium(II) complexes: kinetic and mechanistic study

Meshack K. Sitati, Gershom Kyalo Mutua, Daniel O. Onunga, Deogratius Jaganyi & Allen Mambanda

To cite this article: Meshack K. Sitati, Gershom Kyalo Mutua, Daniel O. Onunga, Deogratius Jaganyi & Allen Mambanda (2021) The effect of substituents on the reactivity of dichloridotriphenylphosphinoruthenium(II) complexes: kinetic and mechanistic study, Journal of Coordination Chemistry, 74:9-10, 1349-1365, DOI: 10.1080/00958972.2021.1904234

To link to this article: https://doi.org/10.1080/00958972.2021.1904234

JOURNAL OF COORDINATION CHEMISTRY
2021, VOL. 74, NOS. 9–10, 1349–1365
https://doi.org/10.1080/00958972.2021.1904234

Taylor & Francis
Taylor & Francis Group

The effect of substituents on the reactivity of dichloridotriphenylphosphinoruthenium(II) complexes: kinetic and mechanistic study

Meshack K. Sitati[a,b], Gershom Kyalo Mutua[a,c], Daniel O. Onunga[a,d], Deogratius Jaganyi[e,f] and Allen Mambanda[a]

[a]School of Chemistry and Physics, University of KwaZulu-Natal, Scottsville, Pietermaritzburg, South Africa; [b]Department of Mathematics and Physical Sciences, Maasai Mara University, Narok, Kenya; [c]Department of Pure and Applied Chemistry, School of Natural Sciences, Masinde Muliro University of Science and Technology, Kakamega, Kenya; [d]Department of Chemistry, Maseno University, Maseno, Kenya; [e]School of Pure and Applied Sciences, Mount Kenya University, Thika, Kenya; [f]Faculty of Applied Sciences, Department of Chemistry, Durban University of Technology, Durban, South Africa

ABSTRACT

The rates of substitution of chloro ligands from a series of ruthenium(II) complexes, [Ru(κ^3-L)(PPh_3)Cl_2] (L = 2,2′:6′,2″-terpyridine, **1**; 4′-(4-methylphenyl)-2,2′:6′,2″-terpyridine, **2**; 4,4′4″-tri-tert-butyl-2,2′:6′,2″-terpyridine, **3**; 4′-(4-chlorophenyl)-2,2′:6′,2″-terpyridine, **4**; 4-chloro-2,2′:6′,2″-terpyridine, **5** and 2,6-bis(2-pyrazolyl)-pyridine, **6**), by thiourea nucleophiles was investigated under *pseudo*-first-order conditions in methanol as a function of nucleophile concentration and temperature. The chloro ligands were substituted in two steps and the reactivity trend was **4** > **5** > **2** > **1** > **6**. Complexes **2** and **3** having donor substituents on the 2,2′:6′,2″-terpyridine backbone experience a *trans*-effect making them more reactive than **1**. Complexes **4** and **5** are more reactive than **1** due to enhanced π-back-bonding brought about by electron-withdrawing substituents on their 2,2′:6′,2″-terpyridine backbones. The reactivity of **4** is higher than **5** due to greater electron acceptor-ability of the chlorophenyl substituent than the chloro substituent in **5**. The 2,6-*bis*(pyrazolyl)pyridine ligand in **6** retards the reactivity of the complex compared to **1** due to the *cis*-donor effect of the pyrazole. The reactivity of the complexes is associative for all nucleophiles in step one and only thiourea in step two. The substitution reactions proceed by a steady changeover from an associative interchange mechanism (I_a) to a dissociative interchange (I_d) mechanism on increasing steric hindrance.

ARTICLE HISTORY
Received 1 August 2020
Accepted 18 February 2021

KEYWORDS
Cis-effect; kinetics; ruthenium(II); substitution; thiourea; trans-effect

CONTACT Meshack K. Sitati meshacksitati@gmail.com School of Chemistry and Physics, University of KwaZulu-Natal, Private Bag X01, Scottsville, Pietermaritzburg 3209, South Africa; Deogratius Jaganyi deojaganyi@gmail.com School of Pure and Applied Sciences, Mount Kenya University, P.O. Box 342-01000, Thika, Kenya.

Supplemental data for this article can be accessed here.

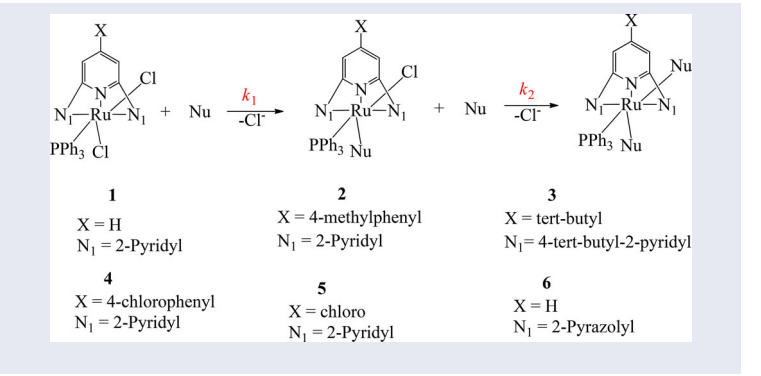

1. Introduction

The coordination chemistry of Ru(II) has been a focus due to its versatile applications, particularly in the area of DNA intercalation and protein binding [1]. Tridentate ligands such as 2,2′:6′,2″-terpyridine (tpy) and its derivatives have been used extensively by Metcalfe *et al.* in the synthesis of Ru complexes [2]. The tpy ligand and its derivatives have been widely studied as chelating ligands because they form strong σ-bonds with metals forming complexes with many applications [3]. The tpy type ligands have also shown cytotoxicity against several human tumor cell lines [4]. A number of complexes incorporating these ligands have been reported to interact with DNA through electrostatic interaction, intercalation, and groove binding [5].

Many Ru(tpy) complexes are potent DNA intercalators. For example, the activity of tpyRu(III)Cl_3 against L1210 leukemia cells compares favorably to that of *cis*platin [6]. The physical and chemical properties and DNA binding capacity of Ru(tpy) complexes and hence their interaction with DNA can be varied by the introduction of different substituents on the tpy ligand [7]. Turro and coworkers reported DNA photo-cleavage by Ru(tpy)-3-(pyrid-2-yl)dipyrido(3,2,-a:2′,3′-c)phenazine in the presence of oxygen [8]. The substituent ensured favorable intercalating interactions by the planar groups at the sites of DNA cleavage. Complexes incorporating tpy and N-N bidentate ligands like $[Ru(tpy)(bipyridine)O]^{2+}$ and $Ru(tpy)(bipyridine)OH]^{2+}$ were also found to be efficient DNA photocleaving agents [9]. The DNA cleavage of [Ru(tpy)*N*,*N*,*N*,*N*-tetramethylenediamine)$OH_2]^{2+}$ was also confirmed by cyclic voltammetry [10–12].

The complexes $[Ru(\kappa^3\text{-}L)(PPh_3)_2\text{-}Cl]^+$ (L = tpy or 2,4,6-tris(2-pyridyl)-1,3,5-triazine ligands) have been reported to have bio-catalytic properties [13]. Replacement of one of the triphenyl phosphine ligands by a chloro ligand gave Ru(II) complexes, $[Ru(\kappa^3\text{-}L)(PPh_3)Cl_2]$ (L = tpy or 2,4,6-tris(2-pyridyl)-1,3,5-triazine ligands) which lowers the steric hindrance and increases DNA binding [1]. Data on the biochemical interactions of $[Ru(\kappa^3\text{-}L)(PPh_3)_2\text{-}Cl]^+$ and similar complexes cover mainly their binding interaction with DNA yet potential anticancer metal complexes interact with all sorts of bio-nucleophiles in a biological environment. Investigating the reactivity of the compounds with biomolecules helps in understanding their behavior in biological systems. Understanding their stability, the nature of interactions and the general desire to

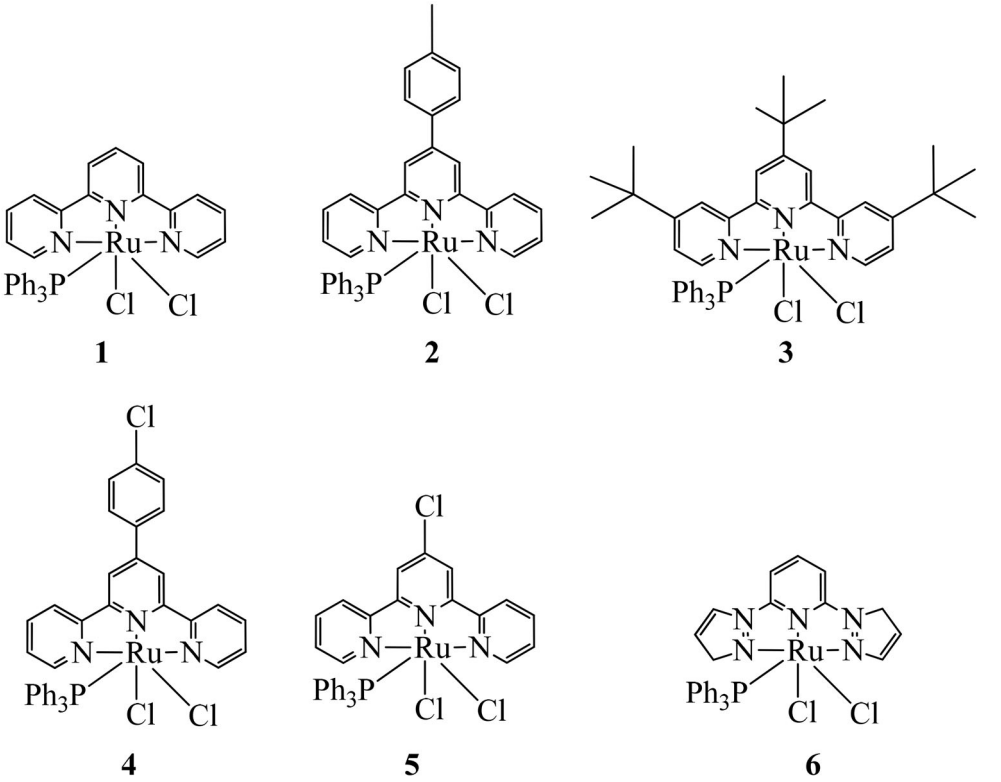

Figure 1. Chemical structure of the neutral ruthenium(II) complexes studied.

investigate the role played by varying the nature of substituents attached at the 4-position of the tpy ligand on the rate of chloro substitution reactions from the neutral Ru(II) complexes motivated this study. The general formula of the compounds of interest is $[Ru(\kappa^3\text{-L})(PPh_3)Cl_2]$ (where L = 2,2′:6′,2″-terpyridine, **1**; 4′-(4-methylphenyl)-2,2′:6′,2″-terpyridine, **2**; 4,4′4″-tri-tert-butyl-2,2′:6′,2″-terpyridine, **3**; 4′-(4-chlorophenyl)-2,2′:6′,2″-terpyridine, **4**; 4-chloro-2,2′:6′,2″-terpyridine, **5** and 2,6-bis(2-pyrazolyl)pyridine, **6**). The chemical structures of the complexes investigated are shown in Figure 1. Neutral thiourea-based nucleophiles of different steric properties were used, thiourea (TU), 1,3-dimethylthiourea (DMTU) and *1,1,3,3*-tetramethylthiourea (TMTU).

Information on the rate of substitution of potential anticancer agents is important to infer their interactions with biological nucleophiles. In addition to the experimental studies, computational studies were performed using Gaussian 09 W program suite to gain insight into the stereo-electronic properties of the complexes.

2. Experimental

2.1. Materials

Solvents and other reagents such as 2,2′:6′,2″-terpyridine, 4′-(4-methylphenyl)-2,2′:6′,2″-terpyridine,4,4′4″-tri-tert-butyl-2,2′:6′,2″-terpyridine, 4′-(4-chlorophenyl)-2,2′:6′,

2′′-terpyridine, 4-chloro-2,2′:6′,2′′-terpyridine, 2,6-bis(2-pyrazolyl)pyridineand*tris*(triphenylphosphine)-Ru(II)dichloride were purchased from Sigma Aldrich and used as received.

2.2. Syntheses of the complexes

The syntheses of the complexes were carried out according to a modified standard literature method [1, 14].

Dichloro(2,2′:6′,2′′-terpyridine)(triphenylphosphino)ruthenium(II) (**1**). 2,2′:6′,2′′-Terpyridine (46.65 mg, 0.2 mmol) and *tris*(triphenylphosphine)Ru(II)dichloride (191.77 mg, 0.2 mmol) were mixed in 30 mL of benzene and the mixture heated under reflux for 6 h. After cooling to room temperature, the precipitate was collected by filtration, washed several times with cold benzene and diethyl ether then dried under vacuum. Yield: 90.11 mg (67.5%), brown solid. ^{1}H NMR (400 MHz, DMF-d_7, ppm): $\delta = 9.51$ (d, 2H); 8.44 (m, 2H); 8.07 (t, 2H); 7.80 (m, 1H); 7.72 (t, 2H); 7.54 (m, 8H); 7.39 (m, 9H). ^{31}P NMR (400 MHz, DMF-d_7, ppm): $\delta = 41.18$. ^{13}C NMR (400 MHz, DMF-d_7, ppm): $\delta = 121.98, 126.36, 128.39, 132.77, 135.90, 154.49, 159.93$. TOF MS-ES$^+$, *m/z*: 632 $[(\text{M-Cl}^-)]^+$, 710 $\{[(\text{M-Cl}^-)]^+ + \text{DMSO}\}$. Anal. Calcd for $C_{33}H_{26}Cl_2N_3PRu{\cdot}2.5H_2O$ (%): C, 55.62; N, 5.90; H, 4.39. Found: C, 55.64; N, 5.99; H, 4.17.

Dichloro(4′-(4-methylphenyl)-2,2′:6′,2′′-terpyridine)(triphenylphosphino)ruthenium (II) (**2**). Complex **2** was synthesized in the same way as **1** using 4′-(4-methylphenyl)-2,2′:6′,2′′-terpyridine (64.67 mg, 0.2 mmol) and *tris*(triphenylphosphine)Ru(II)dichloride (191.77 mg, 0.2 mmol). Yield: 109.86 mg (72.5%), red-brown solid. ^{1}H NMR (400 MHz, DMF-d_7, ppm): $\delta = 9.36$ (d, 2H); 8.67 (m, 2H); 8.51 (d, 2H); 8.41 (s, 2H); 7.94 (m, 9H); 7.58 (t, 2H); 7.43 (t, 6H); 2.47 (s, 3H). ^{31}P NMR (400 MHz, DMF-d_7, ppm): $\delta = 40.67$. ^{13}C NMR (400 MHz, DMF-d_7, ppm): $\delta = 20.51, 119.51, 122.31, 126.18, 127.35, 127.7, 129.05, 129.84, 132.37, 132.7, 132.96, 134.92, 135.7, 139.19, 143.25, 154.37, 159.86$. TOF MS-ES$^+$, *m/z*: 722 $[(\text{M-Cl}^-)]^+$, 800 $\{[(\text{M-Cl}^-)]^+ + \text{DMSO}\}$. Anal. Calcd for $C_{40}H_{32}Cl_2N_3PRu{\cdot}2H_2O$ (%): C, 60.52; N, 5.29; H, 4.57. Found: C, 60.13; N, 5.29; H, 4.46.

Dichloro(triphenylphosphino)(4,4′,4′′-tri-tert-butyl-2,2′:6′,2′′terpyridine)ruthenium (II) (**3**). Complex **3** was synthesized in the same way as **1** using 4,4′,4′′-tri-tert-butyl-2,2′:6′,2′′-terpyridine (80.31 mg, 0.2 mmol) and *tris*(triphenylphosphine)Ru(II)dichloride (191.77 mg, 0.2 mmol). Yield: 104.48 mg (62.5%), red solid. ^{1}H NMR (400 MHz, DMF-d_7, ppm): $\delta = 9.16$ (d, 2H); 8.85 (d, 2H); 8.24 (s, 2H); 7.52 (d, 9H); 7.28 (m, 3H); 7.14 (t, 2H); 1.38 (m, 27H). ^{31}P NMR (400 MHz, DMF-d_7, ppm): $\delta = 43.71$. ^{13}C NMR (400 MHz, DMF-d_7, ppm): $\delta = 29.47, 34.61, 119.30, 123.01, 127.61, 128.66, 132.83, 153.74, 155.69, 159.5, 165.03$. TOF MS-ES$^+$, *m/z*: 835 ($M^+$). Anal. Calcd for $C_{45}H_{50}Cl_2N_3PRu$ (%): C, 64.66; N, 5.03; H, 6.03. Found: C, 64.51; N, 5.14; H, 6.33.

Dichloro(4′-(4-chlorophenyl)-2,2′:6′,2′′-terpyridine)(triphenylphosphino)ruthenium (II) (**4**). Complex **4** was synthesized in the same way as **1** using 4′-(4-chlorophenyl)-2,2′:6′,2′′-terpyridine (68.76 mg, 0.2 mmol) and *tris*(triphenylphosphine)Ru(II)dichloride (191.77 mg, 0.2 mmol). Yield: 109.71 mg (70.5%), red solid. ^{1}H NMR (400 MHz, DMF-d_7,

ppm): $\delta = 9.55$ (d, 2H); 8.67 (d, 2H); 8.61 (s, 2H); 8.30 (d, 2H); 8.11 (m, 2H); 7.86 (t, 2H); 7.76 (t, 2H); 7.59 (m, 6H); 7.38 (m, 9H). ^{31}P NMR (400 MHz, DMF-d_7, ppm): $\delta = 40.29$. ^{13}C NMR (400 MHz, DMF-d_7, ppm): $\delta = 119.79$, 122.53, 126.44, 127.97, 129.34, 132.85, 134.62, 135.92, 136.82, 141.80, 154.52, 160.07. TOFMS-ES$^+$, *m/z*: 742 [M^+], 820 [M^+ + DMSO]. Anal. Calcd for $C_{39}H_{29}Cl_3N_3PRu$ (%): C, 60.20; N, 5.40; H, 3.76. Found: C, 59.90; N, 5.31; H, 4.15.

Dichloro(4-chloro-2,2′:6′,2″-Terpyridine)(triphenylphosphino)ruthenium(II) (**5**). Complex **5** was synthesized in the same way as **1** using 4-chloro-2,2′:6′,2″-terpyridine (53.54 mg, 0.2 mmol) and *tris*(triphenylphosphine)Ru(II)dichloride (191.77 mg, 0.2 mmol). Yield: 83.67 mg (59.6%), red solid. ^{1}H NMR (400 MHz, DMF-d_7, ppm): $\delta = 9.39$ (d, 2H); 8.40 (d, 2H); 8.29 (s, 2H); 7.96 (t, 2H); 7.63 (t, 6H); 7.42 (m, 9H); 7.29 (m, 2H). ^{31}P NMR (400 MHz, DMF-d_7, ppm): $\delta = 39.39$. ^{13}C NMR (400 MHz, DMF-d_7, ppm): $\delta = 122.40$, 126.80, 127.89, 132.91, 135.93, 137.06, 154.42, 158.74, 160.96. TOF MS-ES$^+$, *m/z*: 703 (M^+). Anal. Calcd for $C_{33}H_{25}Cl_3N_3PRu$ (%): C, 56.46; N, 5.99; H, 3.59. Found: C, 56.80; N, 6.33; H, 3.20.

Dichloro(2,6-bis(2-pyrazolyl)pyridine)(triphenylphosphino)ruthenium(II) (**6**). Complex **6** was synthesized in the same way as **1** using 2,6-bis(2-pyrazolyl)pyridine (42.64 mg, 0.2 mmol) and *tris*(triphenylphosphine)Ru(II)dichloride (191.77 mg, 0.2 mmol). Yield: 56.07 mg (43.3%), yellow solid. ^{1}H NMR (400 MHz, DMF-d_7, ppm): $\delta = 9.79$ (d, 1H); 9.02 (m, 4H); 7.95 (m, 9H); 7.69 (m, 2H); 7.43 (m, 6H); 6.36 (m, 2H). ^{31}P NMR (400 MHz, DMF-d_7, ppm): $\delta = 50.34$. ^{13}C NMR (400 MHz, DMF-d_7, ppm): $\delta = 106.61$, 110.33, 128.42, 130.13, 132.75, 137.51, 162.27. TOF MS-ES$^+$, *m/z*: 610 [(M-Cl$^-$)]$^+$. Anal. Calcd for $C_{29}H_{26}Cl_2N_5PRu$ (%): C, 53.96; N, 10.85; H, 4.05. Found: C, 53.80; N, 10.84; H, 3.90.

All the complexes gave ^{1}H, ^{31}P, and ^{13}C NMR spectra corresponding to the proposed structures and elemental analysis data consistent with their formulations. Mass spectrometric data gave peaks corresponding to the masses of the complexes. The NMR and MS spectra are placed in the Supporting Information (Figures S1–S24).

2.3. Instrumentation and measurements

NMR spectra were recorded on a Bruker Avance DPX 400 MHz Spectrophotometer at 303 K using $Si(CH_3)_4$ as a reference. Low resolution electron spray ionization (ESI$^+$) mass spectra were recorded on the Waters Micromass LCT Premier Spectrometer or Shimadzu LCMS 2020. Elemental analyses were done on a ThermoScientific Flash 2000 elemental analyser. Kinetic measurements for fast reactions were performed on an Applied Photophysics SX20 Stopped Flow instrument coupled with an online data acquisition system whose temperature is controlled within ±0.1 °C. The slow reactions were monitored using a Varian Cary 100 Bio Ultraviolet-Visible Spectrophotometer with an attached Varian Peltier temperature controller and online kinetic application. The Ultraviolet-Visible Spectrophotometer was also used to pre-determine the wavelengths at which the reactions were monitored.

2.4. Kinetic measurements

The rate of substitution was measured under *pseudo*-first-order conditions. Kinetic solutions were prepared by dissolving the required amount of complex in 0.1 M ionic solution consisting of 0.01 M LiCl and 0.09 M $NaClO_4$ in dry methanol to achieve a specific concentration. The chloride from LiCl suppressed any possibility of solvolysis of the complexes. The perchlorate ion is a poor nucleophile and cannot competitively substitute the co-labile ligand ahead of the incoming thiourea ligands [15]. Nucleophile stock solutions were prepared at 100 times higher than the concentration of the respective complex and diluted to afford concentrations of 80, 60, 40, and 20 times. Equal volumes of nucleophile and metal compound solutions are mixed and the change in absorbance with time of the solution mixture studied. The reaction comes to an end when the absorbance no longer changes with time. The time taken for absorbance *versus* time curve to flatten which is obtainable from the OriginPro 9.1 software gives the time the reaction takes to come to an end. The inverse of the time(s) taken to complete a reaction gives the observed rate constant.

2.5. Computational modelling

Computations were done by Density Functional Theory (DFT) run on Gaussian 09 suite of programs [16]. The structures were optimized using the hybrid Becke, 3-parameter, Lee-Young-Parr method of Los Alamos National Laboratory 2 double ζ basis sets having inner core electrons of the Ru replaced by relativistic effective core potential [17]. DFT applies to physically observable electron density over a wave function in determination of the properties of a system. Los Alamos National Laboratory 2 double ζ basis set exploits relativistic effective core potentials to account for effect of inner core 28 electrons ([Ar]$3d^{10}$) in Ru [18]. To take into account of the solvent effects, the complexes were fully optimized in methanol using the conductor polarizable continuum model [19]. The singlet state was used due to the low electronic spin state of the Ru(II) complexes. The chemical potential (μ) and molecular hardness (η) for each structure were calculated from the HOMO and LUMO energies. The global electrophilicity indices (ω) were determined by the relationship $\omega = \mu^2/2\eta$ [20]. The charge on each atom is expressed as natural bond orbitals (NBO) [21].

3. Results

3.1. Computational results

DFT calculated quantities (Table 1) have been used to explain kinetic behavior [22]. For example, electronic chemical potential, μ, chemical hardness, η, and electrophilicity index, ω, have been used to support observed trends in the rates of substitution reactions [23]. In this study, calculations and optimization were carried out to gain information on the electronic and structural properties of the complexes. The DFT optimized structures of the complexes are shown in Table 2 and a summary of selected DFT results are presented in Table 1. The DFT calculated frontier molecular orbitals (Table 2) show that the HOMO is located mainly on Ru and partially on the

Table 1. Summary of DFT calculated data for the complexes investigated.

Parameters	1	2	3	4	5	6
Distances (Å)						
Ru22-Cl23	2.58	2.59	2.59	2.59	2.57	2.56
Ru22-Cl25	2.56	2.55	2.56	2.48	2.55	2.56
Ru22-N39	1.97	1.97	1.97	1.97	1.96	1.99
Ru22-N40	2.10	2.10	2.10	2.10	2.10	2.10
Ru22-N41	2.10	2.10	2.10	2.10	2.10	2.10
Angles (°)						
N41-Ru22-N40	159.2	159.0	158.6	159.1	159.1	157.9
N40-Ru22-N39	79.8	79.7	79.5	79.8	79.8	79.3
Cl23-Ru22-Cl25	89.4	89.7	89.7	89.3	89.4	90.2
NBO charges (eV)						
Ru(22)	0.171	0.164	0.151	0.176	0.173	0.133
Orbital energy (eV)						
HOMO	−5.488	−5.471	−5.360	−5.525	−5.571	−5.620
LUMO	−2.479	−2.514	−2.289	−2.568	−2.604	−2.180
$\Delta E_{\text{HOMO-LUMO}}$	3.009	2.957	3.070	2.957	2.967	3.440
Global chemical reactivity indices						
η (eV)	1.504	1.478	1.535	1.484	1.478	1.720
μ (eV)	−3.984	−3.992	−3.824	−4.088	−4.047	−3.900
ω (eV)	5.275	5.389	4.763	5.633	5.539	4.422

η: chemical hardness; μ: electronic chemical potential; ω: electrophilicity index.

chloro ligands while the LUMO is on the N-N-N ligands as has also been observed [24]. Figure 2 shows typical numbering of the atoms in the complexes.

The HOMO-LUMO energy gap has been used to predict kinetic stability and chemical reactivity of the compounds. Compounds with wider energy gap (Table 1) are likely to be kinetically stable and chemically less reactive [25]. The coordination geometry about the Ru(II) in these complexes (Figure 1) is distorted octahedral. The angle N40-Ru22-N39 (79.8°) and N41-Ru22-N40 (159.2°) is smaller than the expected 90° and 180°, respectively. The Cl23-Ru22-Cl25 angle is 90° confirming that the chloro groups are *cis*. The DFT calculated results in Table 1 are in agreement with the literature findings on similar Ru(II) complexes [26]. The DFT results reveal that the distances of the axial nitrogens from Ru(II) (Ru22-N39) are shorter than those of the equatorial ones (Ru22-N40/41). This further attests to the distortion in the coordination geometry of the Ru(II) complexes.

3.2. Kinetic results

The rate of substitution of the chloro ligands was measured spectrophotometrically by following the change in absorbance with time using an Ultraviolet-Visible Spectrophotometer for slow reactions or a Stopped Flow spectrophotometer for fast reactions. Spectral changes due to the reactions were observed from 200 to 800 nm to establish a suitable wavelength at which the respective reaction for each metal complex could be followed. All reactions were thermostated within ± 0.1 °C of the set value. The changes in absorbance accompanying the reactions were analyzed graphically using OriginPro 9.1 software. Kinetic traces were taken at appropriate wavelength and fitted to a single exponential decay standard function to generate *pseudo*-first order rate constants (k_{obs}) using equation (1):

$$A_t = A_o + (A_o - A_\infty) \exp(-k_{\text{obs}} t) \quad (1)$$

Table 2. DFT Minimum energy structures and frontier molecular orbitals of the complexes.

Optimized structures		HOMO	LUMO
	1	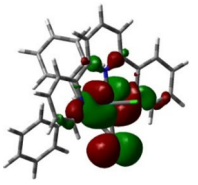	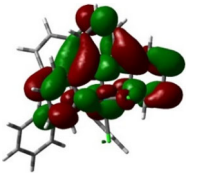
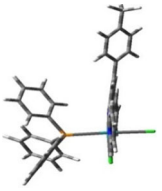	2	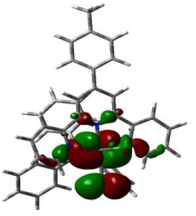	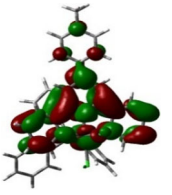
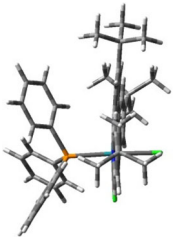	3	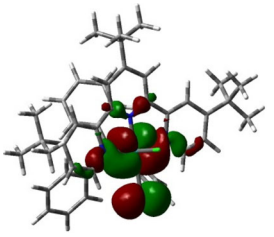	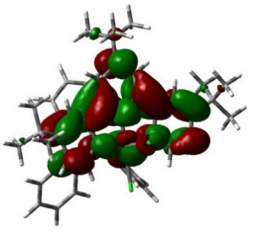
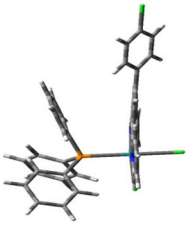	4	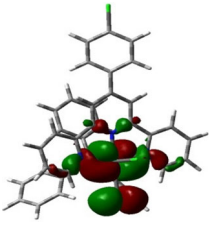	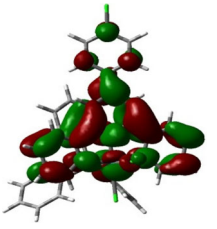
	5	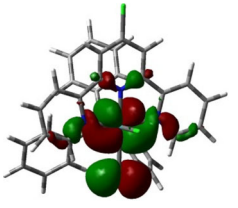	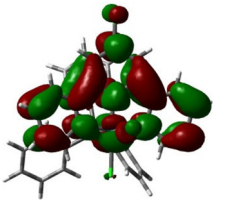
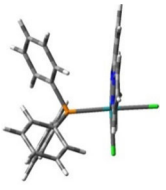	6	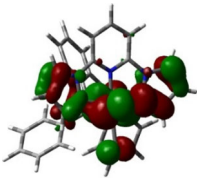	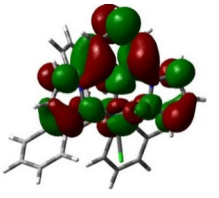

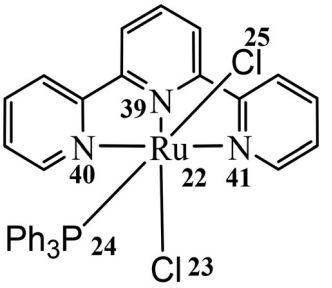

Figure 2. Structure of **1** illustrating numbering of atoms and the spatial orientation of the ligands around the Ru(II) metal center.

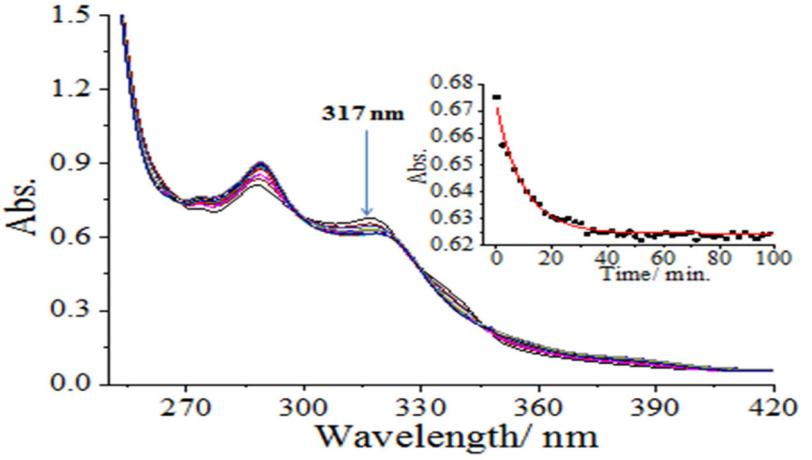

Figure 3. Absorbance spectra for the reaction of **4** and DMTU on the UV visible spectrophotometer at 298 K (*inset* is the kinetic trace obtained for the reaction at 317 nm).

where A_o = absorbance at the commencement of the reaction, A_t = absorbance at time t, and A_∞ = absorbance at the end of the reaction [15]. An example of such spectral changes for the reaction of **4** with DMTU is shown in Figure 3.

The rate of nucleophilic attack by the thiourea nucleophiles was calculated from the observed rate constant measured by varying the concentration of the nucleophile at 25 °C. The average values of the observed rate constant, $k_{obs/obs'}$, for the first or second step of the reaction were plotted against [Nu]. Linear plots of $k_{obs/obs'}$ *versus* [Nu] were obtained for all reactions and typical plots are shown in Figure 4 for the substitution reactions of **3** with the thiourea nucleophiles at 25 °C.

The slopes represent the second order rate constants, k_2 (a) and $k_{2'}$ (b), respectively. Other similar plots are placed in Supporting Information (Figures S25, S26, S28, S29, S31, S33, S34, and S36). Tables of $k_{obs/obs'}$ and respective nucleophile concentrations are presented in Supporting Information (Tables S1, S2, S5, S6, S9, S10, S17, and S18).

3.3. Confirmation of substitution mechanism by ^{31}P NMR

The ^{31}P NMR spectra in Figure 5 illustrate the substitution from **2** by the thiourea nucleophile. The ^{31}P NMR spectrum of **2** before reaction shows a single chemical shift

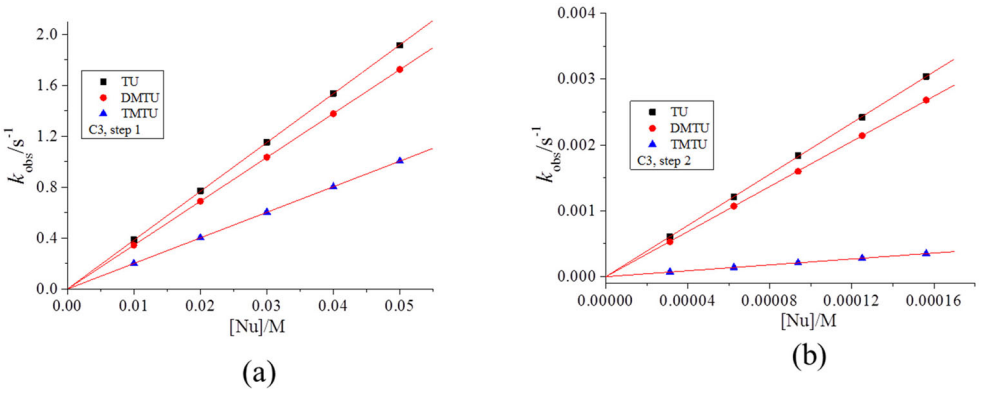

Figure 4. Plots of k_{obs} (a) and $k_{obs'}$ (b) *vs.* [Nu] for the reactions of **3** with the thiourea nucleophiles at 298 K.

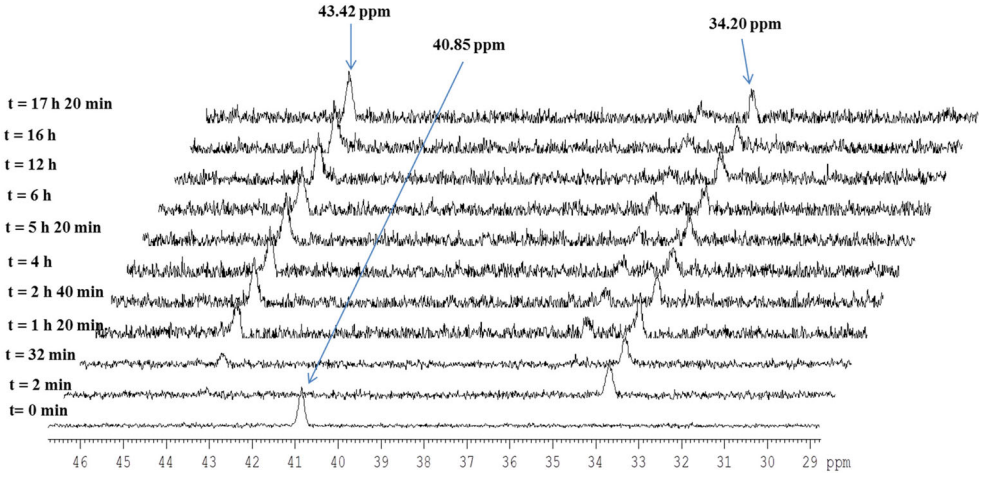

Figure 5. ^{31}P NMR spectral array for the reaction of **2** with thiourea (TU).

at 40.85 ppm. On mixing the complex with TU, a new peak at 34.2 ppm appears within 2 min with a concomitant disappearance of the 40.85 ppm resonance peak. The first chloro substitution from **2** produced an intermediate coordinated with one chloro and TU ligand. This intermediate reacts with another TU nucleophile at a much slower rate as evidenced by a decrease in its resonance at 34.20 ppm and concomitant growing of a resonance peak at 43.42 ppm after 32 min. This resonance is due to Ru(κ^3-tptz)(PPh_3)TU_2 [27]. The ^{31}P NMR peak characteristic of the free triphenylphosphine ligand (Figure 6) was not observed during the course of the substitution reaction.

Based on the kinetic data and ^{31}P NMR kinetics analysis, the proposed mechanism of chloro substitution in the complexes under investigation is represented in Scheme 1.

The rate constants were also measured from 25 to 45 °C in increments of 5 °C. Graphs of ln$k_{2/2'}$/T *versus* 1/*T* were plotted in accordance with the Eyring equation.

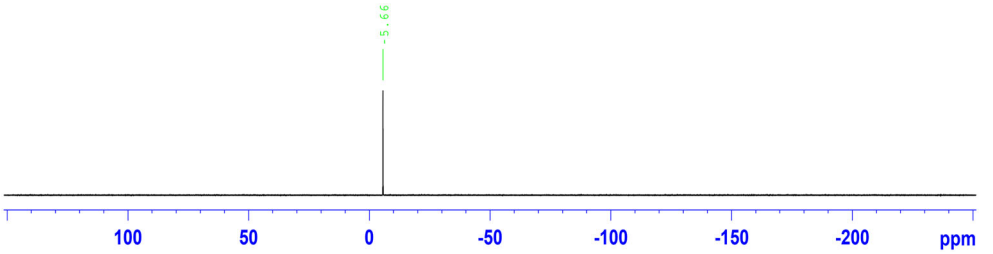

Figure 6. ^{31}P NMR spectra for the free triphenylphosphine ligand.

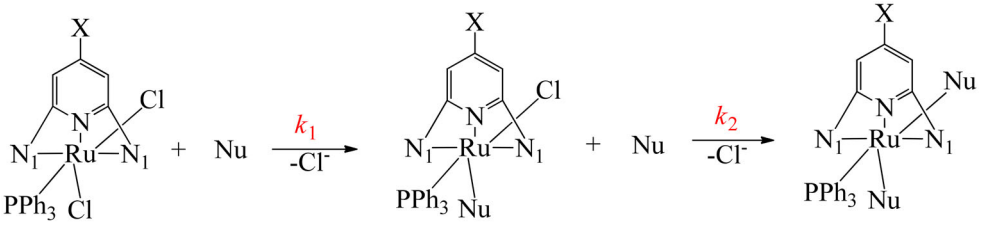

1
X = H
N_1 = 2-Pyridyl

2
X = 4-methylphenyl
N_1 = 2-Pyridyl

3
X = tert-butyl
N_1= 4-tert-butyl-2-pyridyl

4
X = 4-chlorophenyl
N_1 = 2-Pyridyl

5
X = chloro
N_1 = 2-Pyridyl

6
X = H
N_1 = 2-Pyrazolyl

Scheme 1. Proposed mechanisms of substitution of the chloro ligands from the Ru(II) complexes.

Typical Eyring plots are shown in Figure 7 for the reaction of **4** with the thiourea nucleophiles.

Other Eyring plots are presented in Supporting Information Figures S27, S30, S32, and S35. The tables of $\ln(k_2/T)$ and $1/T$ are provided in Supporting Information Tables S3, S4, S7, S8, S15, S16, and S19. The enthalpy of activation ($\Delta H^{\neq}$) and entropy of activation ($\Delta S^{\neq}$) were calculated from the slope and the intercept of the Eyring plots, respectively. The rate constants ($k_{2/2'}$) and activation parameters ($\Delta H^{\neq}$, $\Delta H'^{\neq}$, $\Delta S^{\neq}$, and $\Delta S'^{\neq}$) for the first and second substitution steps are summarized in Tables 3 and 4.

4. Discussion

The stepwise substitutions of the chloro ligands follow the order **3** > **4** > **5** > **2** > **1** > **6**. The differences in the rate of substitution from all the complexes investigated arise from the nature of substituents on the tpy backbone similar to what has been reported for square planar Pt(II) complexes [28]. In analyzing the results, a clear understanding of the role the substituent(s) on tpy ligand is very important because it changes the electronic properties of the ligand, thereby influencing the reactivity of the Ru(II). Both π-back-bonding and σ-*trans* effect have been found to control

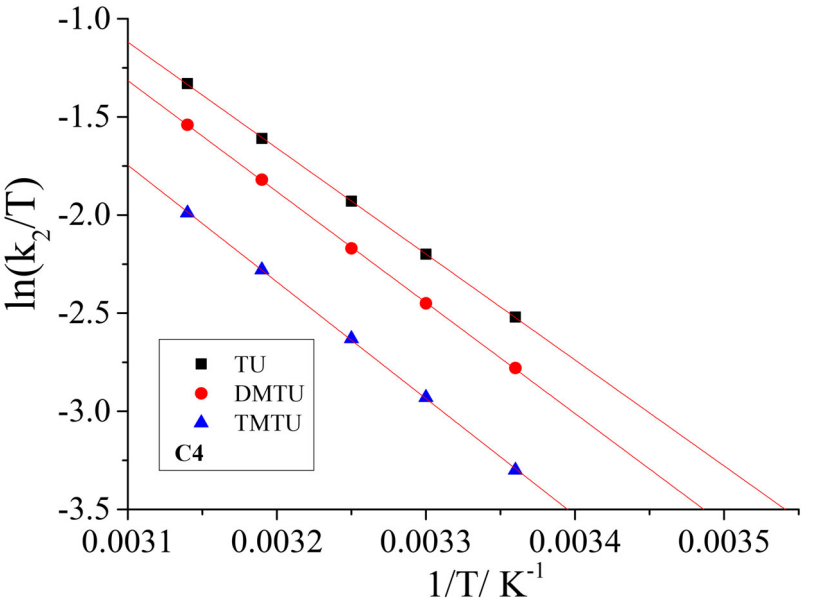

Figure 7. Eyring plots for the reactions of **4** with the thiourea nucleophiles.

reactivity of tpy-Pt(II) complexes depending on the nature of the substituent(s) attached on the tpy [28]. The σ-*trans*-effect and π-back-bonding both alter the rate of substitution in octahedral transition metal complexes [29].

Introduction of the electron-donating methylphenyl substituent [7] at the 4′-position of the tpy ligand in **1** to form **2** and addition of the strongly electron-donating tert-butyl substituents [28] at the 4′-*trans* and *cis* positions of **1** to form **3** results in increased rate of substitution. The increase in the rate of substitution with the addition of electron-donating substituents follows the order **1** < **2** < **3**. The oxidation potentials of these complexes increased as follows: 0.98 V (**3**) < 1.01 V (**2**) < 1.02 V (**1**) [30]. The oxidation potentials inversely correlate to the electron-donating ability of the substituents on the ligands implying highest donation of electrons to Ru(II) in **3** [30].

The trend in the rate of substitution increases in the same way as the electron donor strength, indicating that the reactivity is driven by σ-*trans*-effect where electron density donated to Ru(II) repels the electrons in the chloro ligand and thus weakening the Ru-Cl bond resulting in increased reactivity. The strength of the *trans*-effect increases from **1** to **3** in line with the trend in the reactivity. Evidence in support of increase in electron donation going from **1** to **3** is further indicated by decrease in DFT calculated NBO charges on the Ru metal center in the order 0.171 (**1**) > 0.164 (**2**) > 0.151 (**3**), confirming that **3** is the least electrophilic. Further evidence of electron donation in these complexes is seen in the raising of the HOMO energy as donor effect increases (−5.488 (**1**) < −5.471 (**2**) < −5.360 (**3**)). It has been reported that strong electron donors raise the HOMO energy [31–33]. The very high σ-*trans*-effect in **3** results in unusually high reactivity compared to **1** and **2** which is due to donation of electrons from both *cis* and *trans* positions. The *trans*-effect has been observed in a number of studies [29].

Table 3. Second order rate constants and activation parameters for the first substitution.

Complexes		Nu	k_2 / (M^{-1} s^{-1})	$\Delta H^{\neq}$ / (kJ mol^{-1})	$\Delta S^{\neq}$ / ($Jmol^{-1}$ K^{-1})
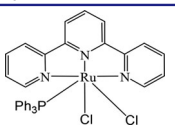	1	TU	19.9 ± 0.3	56 ± 2	−27 ± 5
		DMTU	17.4 ± 0.2	58 ± 1	−22 ± 2
		TMTU	9.7 ± 0.2	67 ± 3	−3 ± 7
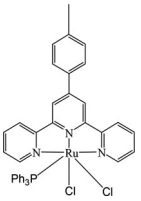	2	TU	26.1 ± 0.2	30 ± 1	−116 ± 3
		DMTU	23.5 ± 0.2	37 ± 2	−96 ± 5
		TMTU	13.8 ± 0.1	58 ± 4	−31 ± 9
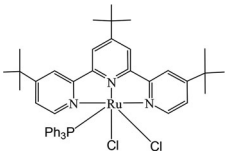	3	TU	38.4 ± 0.4	28 ± 1	−121 ± 4
		DMTU	34.4 ± 0.4	29 ± 3	−118 ± 7
		TMTU	20.5 ± 0.3	55 ± 1	−34 ± 2
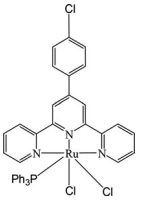	4	TU	23.2 ± 0.4	45 ± 2	−68 ± 6
		DMTU	19.5 ± 0.3	47 ± 1	−63 ± 4
		TMTU	10.4 ± 0.2	61 ± 2	−29 ± 5
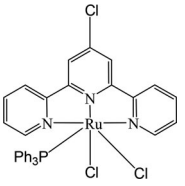	5	TU	22.6 ± 0.2	40 ± 3	−85 ± 7
		DMTU	18.8 ± 0.2	58 ± 1	−90 ± 3
		TMTU	11.4 ± 0.2	60 ± 3	−40 ± 7
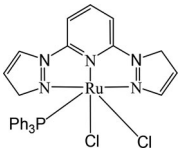	6	TU	0.008 ± 0.0003	80 ± 2	−20 ± 6
		DMTU	0.007 ± 0.0002	90 ± 3	−15 ± 8
		TMTU	0.005 ± 0.0003	120 ± 1	−6 ± 3

The addition of chlorophenyl and chloro ligands at the 4′-position of the tpy ligand in **1** forms **4** and **5**, respectively, resulting in increase in reactivity as follows: **1** < **5** < **4**. A chloro substituent withdraws electron density by π resonance [34] and this enhances the π-back-donation of electron density from the Ru(II) orbitals into the π anti-bonding molecular orbitals of the ligand. Consequently, the positive charge on Ru(II) increases making it more attractive for nucleophilic attack. This observation is supported by the increase in DFT-calculated NBO charges as follows: 0.171 (**1**) < 0.173 (**5**) < 0.176 (**4**). The electrophilicity indices also increase in the same manner (5.275 (**1**) < 5.633 (**4**) < 5.539 (**5**)). This is an indication that **4** and **5** have enhanced π-back-

Table 4. Second order rate constants and activation parameters for the second substitution.

Complexes		Nu	$k_{2'}$ / (10^{-1} $M^{-1}s^{-1}$)	$\Delta H'^{\neq}$ / (kJ mol^{-1})	$\Delta S'^{\neq}$ / (Jmol^{-1} K^{-1})
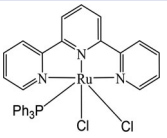	1	TU	108 ± 2	62 ± 1	−24 ± 3
		DMTU	23 ± 0.4	78 ± 2	26 ± 4
		TMTU	2.5 ± 0.2	118 ± 1	140 ± 4
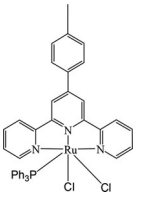	2	TU	166 ± 3	36 ± 3	−99 ± 7
		DMTU	64 ± 2	74 ± 3	19 ± 7
		TMTU	6.5 ± 0.1	106 ± 3	108 ± 9
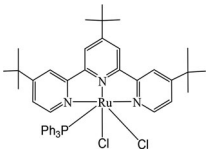	3	TU	195 ± 4	34 ± 2	−102 ± 5
		DMTU	171 ± 2	49 ± 0.3	−58 ± 1
		TMTU	22.4 ± 1	98 ± 0.2	89 ± 1
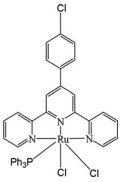	4	TU	143 ± 1	47 ± 2	−59 ± 7
		DMTU	32 ± 0.7	76 ± 0.5	24 ± 1.2
		TMTU	2.7 ± 0.04	112 ± 2	121 ± 5
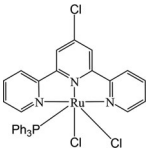	5	TU	113 ± 2	50 ± 3	−56 ± 7
		DMTU	27 ± 0.3	77 ± 2	25 ± 5
		TMTU	2.5 ± 0.02	114 ± 0.3	130 ± 1
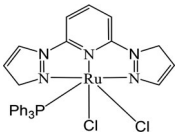	6	TU	0.03 ± 0.002	92 ± 2	−10 ± 6
		DMTU	0.001 ± 0.0001	110 ± 3	28 ± 8
		TMTU	0.0004 ± 0.0001	129 ± 2	146 ± 5

bonding which makes it easier for electron shift from the filled metal Ru *d* orbitals into the empty ligand π^*-orbitals, hence higher reactivity compared to **1**. The fact that **4** is more reactive than **5** indicates that the chlorophenyl substituent is a stronger electron acceptor than the chloro ligand, in line with what has been observed [35].

Notably, **2** and **4** only differ in the substituent on the phenyl at the 4′-position of the tpy. Complex **2** has an overall electron-donating substituent (methyl substituent) while **4** has electron-accepting substituent (chloro substituent). This is clearly supported by their respective DFT calculated quantities as already discussed. The higher reactivity of **2** compared to **4** shows that *trans*-effect due to the methyl substituent in **2** in this study has a greater effect on the substitution reactions than the π-back-bonding due to the chloro group in **4**. The relative higher influence of *trans*-effect compared to the π-back-bonding effect has been observed in other studies [36].

The replacement of the *cis* positioned pyridyl ligands in **1** with pyrazolyl ligands in **6** resulted in a sharp decrease in reactivity. The replacement of pyridyl ligands lowers the π-back-bonding ability of the overall ligand system, leading to a less electropositive metal center and hence lower reactivity. As shown in the literature, pyrazole ligands are effective donors to transition metals [37]. Further, pyrazole has a lower basicity ($pK_a = 2.47$) compared to pyridine ($pK_a = 5.23$) [38–40] which causes it to bind metals more weakly than pyridine. The donor effect of the pyrazolyl ligands is supported by the lower DFT calculated NBO charge for **6** (0.133) compared to **1** (0.171), confirming that **1** is more electropositive. This is further corroborated by the higher electrophilicity index of **1** (5.275) compared to **6** (4.422). In addition, the HOMO-LUMO energy gap and chemical hardness values for **1** are smaller than those of **6** in support of the higher rate of substitution from **1**. Further, the LUMO of **6** (–2.180) is raised compared to that of **1** (–2.479), making it difficult for π-back-donation. The higher π-back-bonding capabilities of the conjugated pyridine rings in **1** readily accept electron density from the Ru(II) metal center compared to the pyrazole rings that are π-electron rich due to an extra pyrollic-N within the chelate ring and hence better π-donors [41].

The rate constants, k_2' for substitution of the second chloro ligand for all the complexes are lower than those of the first step, k_2, due to decrease in the electrophilicity of the metal center upon coordination of the first thiourea nucleophile in complexes where π-back-bonding is dominant [42]. The reduction of the electrophilicity of Ru(II) results from the donation of electrons by the incoming electron rich thiourea nucleophile to the electron deficient metal center lowering its charge. Further, the coordinated nucleophile introduces steric hindrance at the Ru(II) metal center, hindering the approach of the second incoming nucleophile.

The first substitution occurs at the chloro ligand which is within the plane of the tpy ligand framework, Cl23, followed by Cl25 which is perpendicular to the ligand plane. The chloro ligand, Cl23, being within the plane of the ligand is most influenced by the electronic changes of the tpy ligand. This is supported by DFT calculated bond distances between the metal centers and the chloro ligands showing that Ru-Cl23 bonds are slightly longer than Ru-Cl25 by about 0.03 Å, hence easier to break. In addition, since Cl25 is *trans* to a different type of ligand (triphenylphosphine) [43], the rate of substitution of the chloro ligand varies for a given Ru(II) complex.

Generally, for both k_2 and k_2' the value of the activation enthalpy increases as the bulkiness of the thiourea entering ligand increases, which must be related to the increasing steric hindrance encountered by the entering ligand that increases the activation enthalpy barrier. In terms of the activation entropy, there is a general trend of going from more negative to more positive values on increasing the steric hindrance of the entering thiourea nucleophile. This can be interpreted in terms of a steady changeover from an associative interchange mechanism (I_a) to a more dissociative interchange (I_d) mechanism on increasing steric hindrance [44,45]. The trend in reactivity of the nucleophiles was TU > DMTU > TMTU. This can be accounted for in terms of steric factors where reactivity decreases with increase in steric hindrance of the nucleophile.

5. Conclusion

The rate of substitutions in the current study are electronically driven either through *trans*-effect or π-back-donation effects. The complex groupings **2**, **3** and **4**, **5** are more reactive than **1** because of enhanced *trans*-effect and π-back-donation, respectively. The reactivity of **4** is higher than **5** due to the presence of a chlorophenyl substituent on the tpy ligand in **4** that is a stronger π-acceptor than the chloro ligand in **5**. It has been shown that the *trans*-effect in **2** influences the reactivity more strongly than the π-back-donation in **4**. The *cis* electron donation by 2,6-bis(pyrazolyl)pyridine ligand in **6** significantly retards the reactivity of the Ru(II) compared to that of **1**; hence, it can be used to tune the reactivity of Ru(II) complexes. The reactivity of Ru(II) complexes is more strongly affected by the electron-donating ligands (*trans*-effect) than ligands that enhance π-back-donation. The *tert*-butyl substituents in **3** are very strong donor ligands whose donation from both the *cis* and *trans* positions strongly accelerate the reactions. The trend in the DFT calculated data supports the observed reactivity of the complexes. There is a steady change in mechanism from an associative interchange mechanism (I_a) to a more dissociative interchange (I_d) mechanism on increasing steric hindrance.

Acknowledgments

We thank Mr. Craig Grimmer for his support with the NMR analysis, Mrs. Caryl Janse Van Rensburg for her help with mass spectra and elemental analyses and Shaun Ball with management of the deliveries.

Disclosure statement

No potential conflict of interest was reported by the authors.

Funding

This research was funded by the University of KwaZulu Natal South Africa.

ORCID

Deogratius Jaganyi http://orcid.org/0000-0003-4499-6877
Allen Mambanda http://orcid.org/0000-0002-8113-3643

References

[1] S. Sharma, S.K. Singh, D.S. Pandey. *Inorg. Chem.*, **47**, 1179 (2008).
[2] C. Metcalfe, S. Spey, H. Adams, J.A. Thomas. *J. Chem. Soc., Dalton Trans.*, 4732 (2002).
[3] E.C. Constable. *Adv. Inorg. Chem.*, **30**, 69 (1986).
[4] L.X. Zhao, T.S. Kim, S.H. Ahn, T.H. Kim, E.K. Kim, W.J. Cho, H. Choi, C.S. Lee, J.A. Kim, T.C. Jeong, C.J. Chang, E.S. Lee. *Bioorg. Med. Chem. Lett.*, **11**, 2659 (2001).
[5] K.K. Patel, E.A. Plummer, M. Darwish, A. Rodger, M.J. Hannon. *J. Inorg. Biochem.*, **91**, 220 (2002).
[6] P.M. van Vliet, S.M. Toekimin, J.G. Haasnoot, J. Reedijk, O. Nováková, O. Vrána, V. Brabec. *Inorg. Chim. Acta*, **231**, 57 (1995).
[7] A. Jain, C. Slebodnick, B.S. Winkel, K.J. Brewer. *J. Inorg. Biochem.*, **102**, 1854 (2008).
[8] Y. Liu, R. Hammitt, D.A. Lutterman, R.P. Thummel, C. Turro. *Inorg. Chem.*, **46**, 6011 (2007).

[9] B.T. Farrer, H.H. Thorp. *Inorg. Chem.*, **39**, 44 (2000).
[10] N. Grover, N. Gupta, P. Singh, H.H. Thorp. *Inorg. Chem.*, **31**, 2014 (1992).
[11] C.W. Jiang, H. Chao, H. Li, L.N. Ji. *J. Inorg. Biochem.*, **93**, 247 (2003).
[12] H.Y. Ding, X.S. Wang, L.Q. Song, J.R. Chen, J.H. Yu, B.W. Zhang. *J. Photochem. Photobiol. A*, **177**, 286 (2006).
[13] S. Sharma, M. Chandra, D.S. Pandey. *Eur. J. Inorg. Chem.*, **2004**, 3555 (2004).
[14] B.P. Sullivan, J.M. Calvert, T.J. Meyer. *Inorg. Chem.*, **19**, 1404 (1980).
[15] A. Shaira, D. Jaganyi. *J. Coord. Chem.*, **67**, 2843 (2014).
[16] M. Frisch, G. Trucks, H. Schlegel, G. Scuseria, M. Robb, J. Cheeseman, G. Scalmani, V. Barone, B. Mennucci, G. Petersson. *Gaussian 09, Revision D. 01*, Gaussian, Inc., Wallingford, CT (2009).
[17] P.J. Hay, W.R. Wadt. *J. Chem. Phys.*, **82**, 270 (1985).
[18] M. Okamura, M. Yoshida, R. Kuga, K. Sakai, M. Kondo, S. Masaoka. *Dalton Trans.*, **41**, 13081 (2012).
[19] T.L. Bahers, T. Pauporté, G. Scalmani, C. Adamo, I. Ciofini. *Phys. Chem. Chem. Phys.*, **11**, 11276 (2009).
[20] P.K.; Chattaraj, U.; Sarkar, M.; Elango, R.; Parthasarathi, V.; Subramanian. *J. Chem. Sci.*, **117**, 599 (2005).
[21] OriginLab Corporation. *OriginPro 9.1*. OriginLab Corporation, Northampton, MA (2018).
[22] R.G. Parr, W. Yang. In *Density-Functional Theory of Atoms and Molecules*, Vol. 16, *International Series of Monographs on Chemistry*, Oxford University Press, New York (1989).
[23] R.G. Parr, W. Yang. *J. Am. Chem. Soc.*, **106**, 4049 (1984).
[24] S. Sangilipandi, D. Sutradhar, K. Bhattacharjee, W. Kaminsky, S.R. Joshi, A.K. Chandra, K.M. Rao. *Inorg. Chim. Acta*, **441**, 95 (2016).
[25] S.B. Jensen, S.J. Rodger, M.D. Spicer. *J. Organomet. Chem.*, **556**, 151 (1998).
[26] S.B. Billings, M.T. Mock, K. Wiacek, M.B. Turner, W.S. Kassel, K.J. Takeuchi, A.L. Rheingold, W.J. Boyko, C.A. Bessel. *Inorg. Chim. Acta*, **355**, 103 (2003).
[27] T. Ben-Hadda, C. Mountassir, H.L. Bozec. *Polyhedron*, **14**, 953 (1995).
[28] D. Reddy, K.J. Akerman, M.P. Akerman, D. Jaganyi. *Transition Met. Chem.*, **36**, 593 (2011).
[29] B.J. Coe, S.J. Glenwright. *Coord. Chem. Rev.*, **203**, 5 (2000).
[30] A. Jain, J. Wang, E.R. Mashack, B.S.J. Winkel, K.J. Brewer. *Inorg. Chem.*, **48**, 9077 (2009).
[31] G.K. Mutua, D.O. Onunga, M. Sitati, D. Jaganyi, A. Mambanda. *Inorg. Chim. Acta*, **514**, 119972 (2021).
[32] M. Maestri, N. Armaroli, V. Balzani, E.C. Constable, A.M.W.C. Thompson. *Inorg. Chem.*, **34**, 2759 (1995).
[33] C.A. Mebi. *J. Chem. Sci.*, **123**, 727 (2011).
[34] D. Reddy, D. Jaganyi. *Dalton Trans.*, **6724**, 6724 (2008).
[35] M.M. Milutinović, A. Rilak, I. Bratsos, O. Klisurić, M. Vraneš, N. Gligorijević, S. Radulović, ŽD. Bugarčić. *J. Inorg. Biochem.*, **169**, 1 (2017).
[36] E. Shustorovich, M. Porai-Koshits, Y.A. Buslaev. *Coord. Chem. Rev.*, **17**, 1 (1975).
[37] D.L. Jameson, J.K. Blaho, K.T. Kruger, K.A. Goldsby. *Inorg. Chem.*, **28**, 4312 (1989).
[38] J. Catalan, J. Elguero. In *Advances in Heterocyclic Chemistry*, A.R. Katritzky (Ed.), pp. 187–274, Academic Press, Orlando (1987).
[39] C. Wijnberger, C.L. Habraken. *J. Heterocycl. Chem.*, **6**, 545 (1969).
[40] D.L. Jameson, K.A. Goldsby. *J. Org. Chem.*, **55**, 4992 (1990).
[41] J.M. Holland, J.A. McAllister, C.A. Kilner, M. Thornton-Pett, A.J. Bridgeman, M.A. Halcrow. *J. Chem. Soc., Dalton Trans.*, 548 (2002).
[42] B.B. Khusi, A. Mambanda, D. Jaganyi. *J. Coord. Chem.*, **69**, 2121 (2016).
[43] T. Karlen, P. Dani, D.M. Grove, P. Steenwinkel, G. van Koten. *Organometallics*, **15**, 5687 (1996).
[44] H.K. Mandal, P.K. Ghosh, A. Mahapatra. *Polyhedron*, **29**, 2867 (2010).
[45] G.K. Mutua, R. Bellam, D. Jaganyi, A. Mambanda. *J. Coord. Chem.*, **72**, 2931 (2019).